DOI: 10.1002/cbic.200800623

Crystalline Nanorods as Possible Templates for the Synthesis of Amorphous Biosilica during Spicule Formation in Demospongiae

Enrico Mugnaioli,[a] Filipe Natalio,[b] Ute Schloßmacher,[b] Xiaohong Wang,[c] Werner E. G. Müller,[b] and Ute Kolb*[a]

High-resolution microscopy shows that, during the initial stages of demosponge spicule formation, a primordial crystalline structure is formed within the axial filament. The recently developed electron diffraction tomography technique reveals that the nanorods have a layered structure that matches smectitic phyllosilicates. These intracellular nanorods have been considered as precursors of mature spicules.

Introduction

The genomic regulatory systems that control the formation of extracellular skeletal matter, especially when formed from inorganic material, are difficult to understand. In multicellular animals the skeletons are constituted either of calcium or of silicon-based minerals.[1] The two classes of the phylogenetic oldest metazoan phylum Porifera (sponges), the Hexactinellida and the Demospongiae, form their skeleton from biosilica (reviewed in refs. [2] and [3]). The skeletal elements, which construct the species-specific endoskeleton, are termed spicules; they comprise a complex and filigree morphology.[4] The unique feature of spicule formation is their synthesis, which is mediated enzymatically via silicatein.[5] Among the siliceous sponges, the spiculogenesis in the demosponge *Suberites domuncula* is best understood.[6] These animals contain only megascleres that are grouped to the monactinal tylostyles, or rarely to the diactinal oxeas.[7] It could be shown that the initial stages of spicule formation proceed intracellularly.[8] Because the synthesis of the spicules is a rapid process, the earliest stages of spicule formation can be studied under in vitro conditions in the cell culture system, the primmorphs. These cell aggregates are composed of proliferating and highly differentiating cells,[9] including the spicule-forming sclerocytes that comprise special vesicles in which the primary stages of spicules proceed.[10]

Recently it has been discovered that the formation of the siliceous spicules of Demospongiae proceeds intracellularly and enzymatically (via silicatein–silica protein) and occurs in a matrix-guided manner. To understand the spiculogenesis in Demospongiae (*Suberites domuncula*), microscopic and cell culture (primmorphs) techniques were combined and provided very valuable data regarding this unique biomineralization process. For example, transmission electron microscopic (TEM) analysis has been applied to demonstrate that antibodies that were raised against silicatein react both with the axial filament (intracellularly)[6,7] and also with the organic cylinder that surrounds the growing spicules (extracellularly).[7] Since their description by Bütschli (1901),[11] it is established that the spicules are composed of amorphous silica; however, until now studies could be performed only with those primordial spicules that had a size >0.5 μm width and 5 μm length.

We investigated the presence of nanorods that appear inside the axial filament in the first stages of spicule formation. Such nanofeatures are not accessible by X-ray techniques and can be investigated only by electron microscopy. One major advantage of electron microscopy is the potential to collect imaging and diffraction data sequentially from the same sample. Especially for beam-sensitive, structurally complicated, or embedded particles, electron diffraction data deliver important structural information.[12,13] In this contribution we coupled well-established techniques, such as high-resolution transmission electron microscopy (HRTEM) and electron dispersion X-ray spectroscopy (EDX), to the automated diffraction tomography (ADT) module that was recently introduced by our group.[14,15] This technique consists of a combination of nanoelectron diffraction (NED) with scanning transmission electron microscopy (STEM); it increases the accessibility of problematic samples and allows the collection of 3D electron diffraction data in an automated manner.

[a] *Dr. E. Mugnaioli, Dr. U. Kolb*
Institut für Physikalische Chemie, Johannes Gutenberg-Universität
Welderweg 11, 55099 Mainz (Germany)
Fax: (+49) 6131-3923768
E-mail: kolb@uni-mainz.de

[b] *F. Natalio, U. Schloßmacher, Prof. Dr. W. E. G. Müller*
Institut für Physiologische Chemie
Abteilung Angewandte Molekularbiologie
Johannes Gutenberg-Universität
Duesbergweg 6, 55099 Mainz (Germany)

[c] *Prof. Dr. X. Wang*
National Research Centre for Geoanalysis
26 Baiwanzhuang Dajie, 100037 Beijing (China)

Results

TEM imaging

Low-resolution transmission electron microscopy (LRTEM) shows that nanorods with 20 nm diameter and 200 nm length are present intracellularly in the early and initial stages of axial filament formation (Figure 1 A–C).

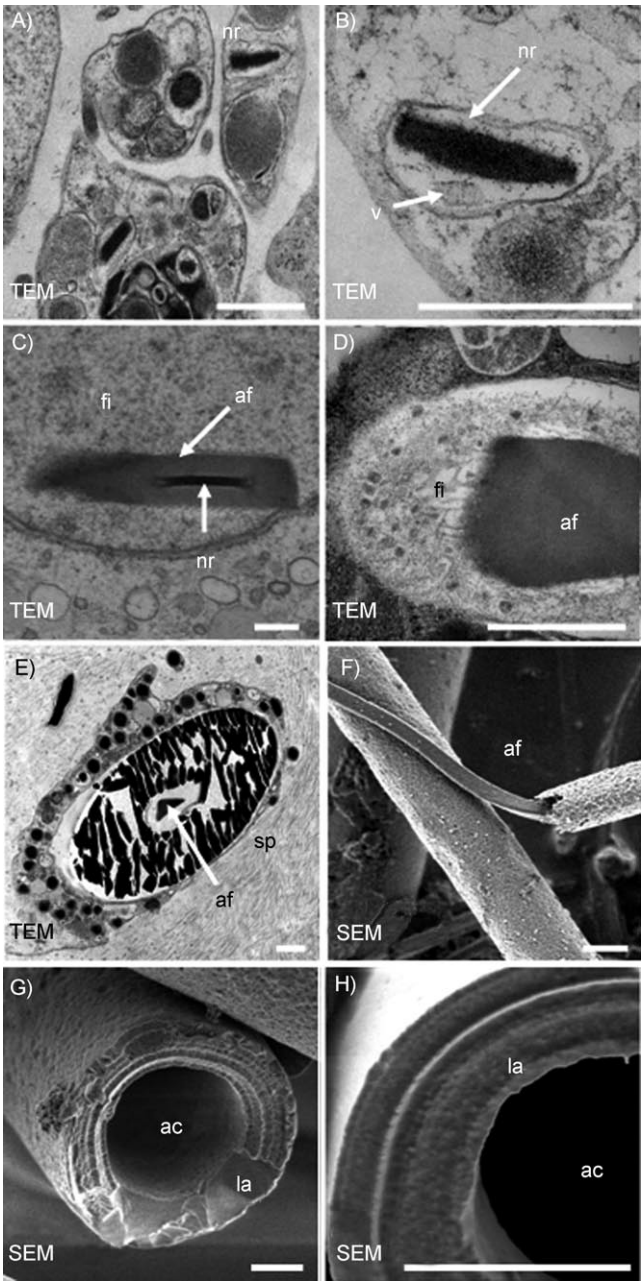

Figure 1. Maturation stages of spicules from *S. domuncula*. A), B) Crystalline nanorod (nr) in a vesicle (v); C) initial formation of an axial filament (af) that comprises a crystalline nanorod (nr); D) the axial filament (af) in a vesicle is linked on one terminus to fibrils (fi) and has lost the crystalline nanorods; E) around the axial filament (af) the first layer of biosilica is produced intracellularly under the formation of an initiating spicule (sp). F) triangular axial filament (af) partly released from mature spicule; G), H) extracellular spicules that had been shortly exposed to HF vapor; the axial canal (ac) is surrounded by appositionally layered biosilica lamellae (la). Bars measure: 500 nm.

The nanorods are then surrounded by a multifunctional polymeric matrix, that is the axial filament and silicatein molecules (Figure 1 C, D). Subsequently, polymeric amorphous biosilica is enzymatically formed concentrically around this axial filament (Figure 1 E). After reaching a size of 7–8 μm in length and of 0.9 μm in diameter, the on-growing spicules are extruded from the cells into the extracellular spaces, where they are completed in size and form by appositional layering of biosilica lamellae (Figure 1 G–H). An axial filament that has been released by short application of HF vapor from a mature spicule is shown in Figure 1 F.

STEM analysis of ultrathin cuts of primmorphs revealed a variety of features with different brightness inside the sponge cells. Among them, selected brighter areas comprise spherical-shape vesicles (silicasomes)[10] and rod-like structures (Figure 2 A, B). These nanorods show a typical size of 300–600 nm

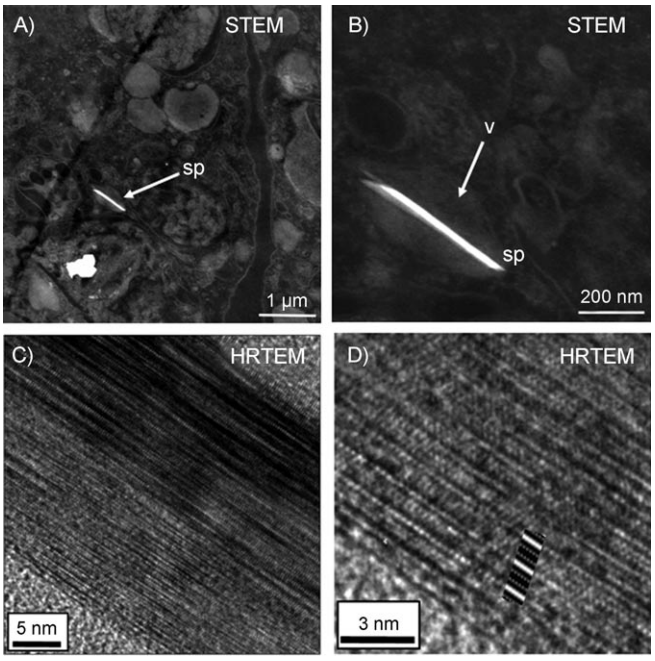

Figure 2. STEM and HRTEM (FFT) analysis of ultra thin stained cuts from primmorphs from *S. domuncula*. A) Overview of a cell (sclerocyte) synthesizing a primordial spicule (sp); B) nanospicule localized intracellularly within a vesicle (v); C), D) HRTEM view down the *b*-axis, with HRTEM image simulated by using the MSLS method at 45 Å thickness.[16]

in length and 20–50 nm in width. Figures 2 A, B show one of these rod-like nanostructures clearly localized within a vesicle inside the sclerocytes. After analyzing different regions of primmorphs by using ultrathin cuts, we found a number of such nanorods, which are always localized intracellularly and never extracellularly.

These nanorods are highly sensitive to electron-beam damage; however, intracellular nanorods from different samples and different areas were analyzed by HRTEM, which revealed a clearly crystalline arrangement (Figures 2 C, D). All the analyzed nanorods show a common layered structure, with a 10 Å distance, arranged parallel to the major growth direction of the rod.

Often several nanorods showing structural defects and bent layers are found within one vesicle. Inside the vesicles, together with nearly single-crystal nanorods, it is possible to observe zigzag or rounded bright features that are completely or partially crystalline (Figure 3). Interestingly, all these features are located intracellularly.

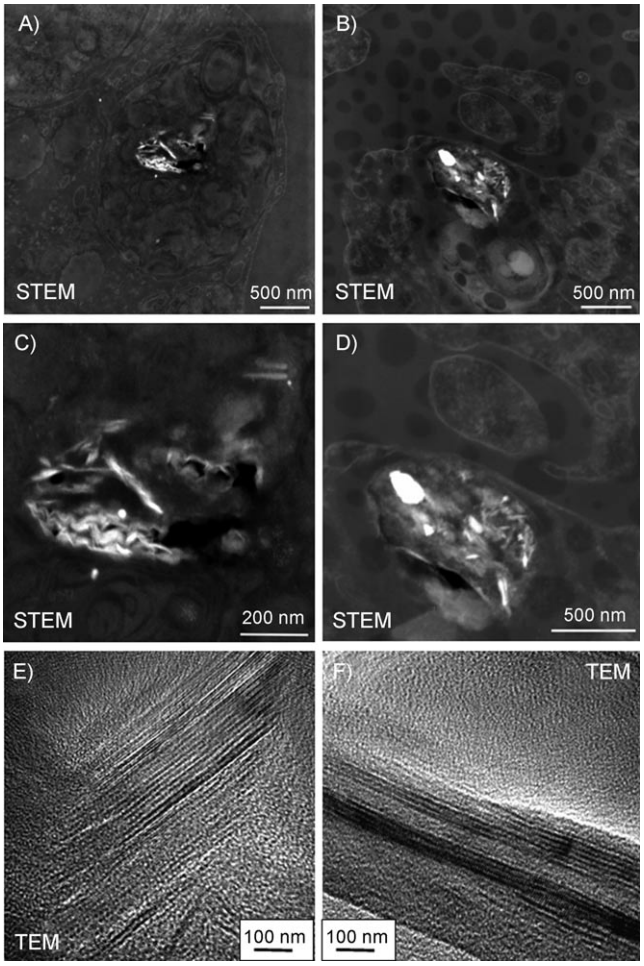

Figure 3. STEM and TEM of primmorphs: A), B) overview C), D) enlarged view of vesicles that contained zig-zag and rounded features; E,F) TEM images showing 10 Å *d*-spacing.

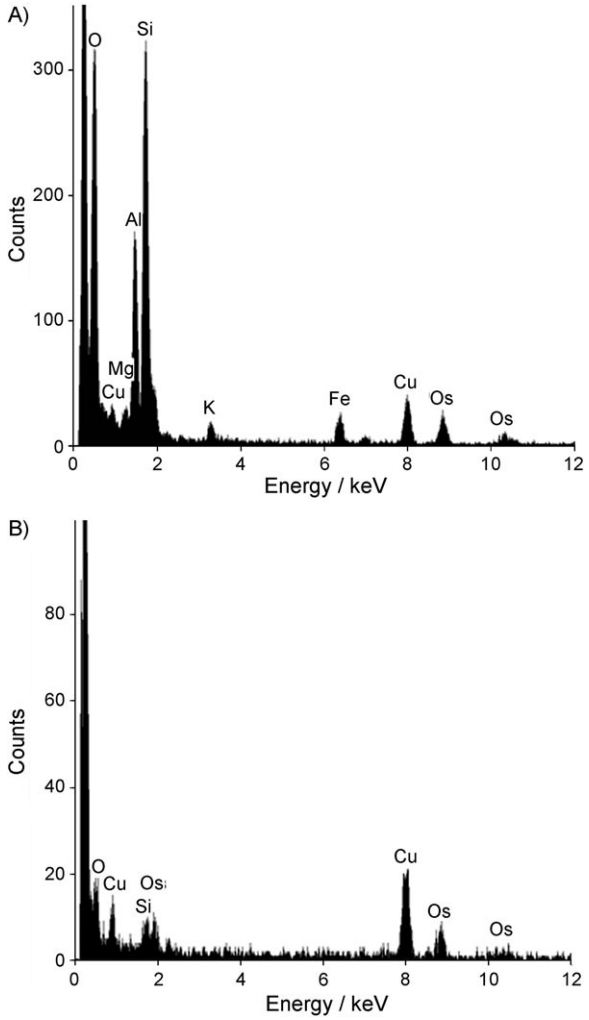

Figure 4. A) EDX spectra of a nanorod: composition (atomic %): O 63.5, Si 21.2, Al 11.5, Mg 1.9, K 0.9, Fe 0.9. B) EDX spectra from the surrounding cell: only small Os, Si and O peaks are detectable from the sample, and the Cu signal comes from the grid.

Chemical analysis

The chemical composition of nanorods was determined by EDX (Figure 4). They are mainly composed by silica and oxygen, but also significant amounts of Al, Mg, K, and Fe are present. The average atomic composition (atomic %) of nanorods is: O 63.5, Si 21.2, Al 11.5, Mg 1.9, K 0.9, Fe 0.9; so, the nanorods do not consist of pure SiO_2, as expected for mature spicules. Their composition is instead close to natural Al-silicate minerals. As a control, EDX analysis of the immediate surrounding environment (cytosol) only showed small signals from Os, Si, and O.

The elements that are detected in nanorods are also concentrated in mature spicules, even if in different proportions. The composition (atomic %) of *S. domuncula* spicules had been determined by ICP-AES to be: O 66.1, Si 32.8, Al 0.006, Mg 0.004, K 0.026, Fe 0.002, Na 1.07, Ca 0.004.

Structural characterization of nanorods

The precise structural characterization of the nanorod shown in Figure 2 was performed by nano-electron diffraction (NED), by using the automated diffraction tomography (ADT) module that was developed recently by our group.[14,15] This module collects slices of the reciprocal space by tilting the particle around the sample holder axis in defined tilt steps. In contrast to the manual tilt data acquisition, this approach does not require a specific orientation of the particle before tilting. In addition, a tilt of $\pm 30^{\circ}$ is sufficient to determine the cell parameters automatically. All the data acquisition, that is, imaging with STEM and diffraction in NED mode, was performed with a low electron dose (3e/Å2s); this implies that no significant beam damage was inflicted on the sample. A 3D reconstruc-

tion of the reciprocal space, which is projected along the tilt axis is shown in Figure 5 A.

C-centring is directly visible in projection [001] in Figure 5 B. In the same figure the presence of a second crystal that is slightly misaligned along c^* is evident. Most of the nanorods analyzed show such defects, as presented in Figure 5 D, which are ubiquitous in layer silicates (phyllosilicates) formed under low-temperature conditions.[17] Even in the presence of these additional spots, the program for automated cell parameter determination was able to find and refine a unit cell with $a=5.18(5)$ Å, $b=9.13(7)$ Å, $c=10.1(3)$ Å, $\beta=96^\circ$. The lattice parameters indicate a layer silicate that is constructed of alternating sheets of Si_2O_5 tetrahedra and $(Al,Mg,Fe)_2(OH)_2$ octahedra.[17,18] The *d*-spacing of 10 Å indicates a TOT–TOT stacking sequence. In particular, lattice parameters fit the cell of a single-layer smectite (space group C2/m, $a=5.2$ Å, $b=9.2$ Å, $c=10$–14 Å, $\beta=99$–100°).[18,19]

By recalculating the number of cations for eleven oxygen atoms from the EDX analysis, we get the following stoichiometry: Si 3.86, Al 2.00, Mg 0.34, K 0.16, Fe 0.16. Such a composition is indeed inside the allowed range for smectites, including montmorillonitic, beidellitic and nontronitic components.[19,20] These types of minerals have been widely identified in marine environments and were occasionally linked to biological activity.[21]

A closer analysis of 3D reconstructed reciprocal space clearly evidences c-axis doubling ($c=20.2$ Å) through the presence of additional reflections for $k\neq 0$ (Figure 5 C); this indicates a two-layer structure with space group *C*2/*c*, as given in Figure 6.

Discussion

The elucidation of the morphology of the spicules has been intensively pursued for more than 250 years, starting with the illustrations of Donati,[22] the descriptions by Carter,[23] and the comprehensive synthesis given by Uriz et al.;[24] however, the mechanism by which silica is concentrated/deposited within and around the spicules as well the early stages of spiculogenesis remained unclear. A major breakthrough was made when it was found that silica/biosilica in this class of sponges is formed enzymatically via the enzyme silicatein.[25,26]

Later on, we could demonstrate that the formation and development of the siliceous spicules in Demospongiae proceeds by an initial synthesis from the central axial filament, which is located in the axial canal, and completed by appositional growth via newly formed layers. By applying the in vitro cell culture system, the primmorphs, it was possible to thoroughly study the rapid synthesis of spicules in *S. domuncula*, by focusing also on the very early stages of growth[8] and it could be unequivocally demonstrated that the initial formation of the spicules starts intracellularly as reported earlier,[24,27,28] and then the spicules are continued and completed extracellularly in the mesohyl.

The HRTEM data presented here show the presence of intracellular nanorods that comprise a crystalline structure. Wilkinson and Garrone described for the first time the presence of an *obvious* crystallinity in the axial filament of raphids and

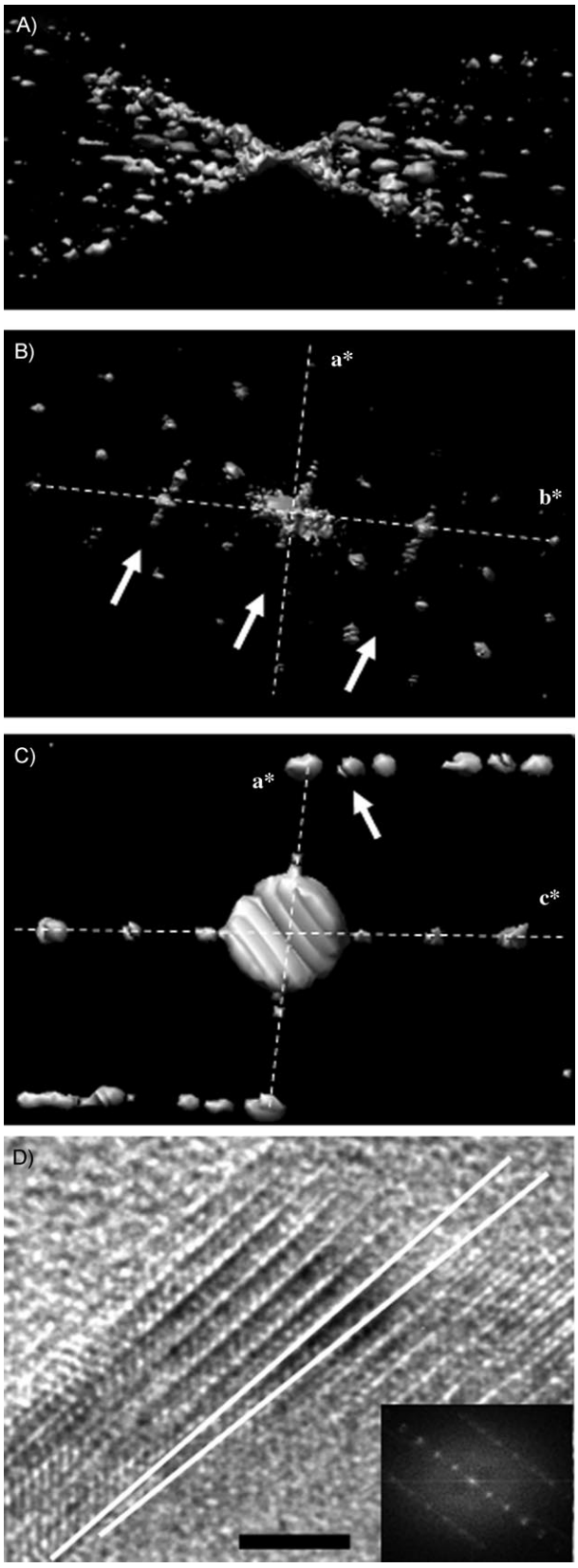

Figure 5. Projections of ADT data from the selected nanorod: A) along tilt axis; B) down c^*-axis, arrows indicate misalignment plane of c^*-axis; C) down the *b*-axis, arrows indicate 20 Å reflections allowed above or below the [010] zone. D) HRTEM and FFT of nanorod to clarify the origin of crystal misalignment along *c*-axis found in ADT data, white lines indicate exemplarily the deviation of *c*-axis. Scale bar (black) is 4 nm.

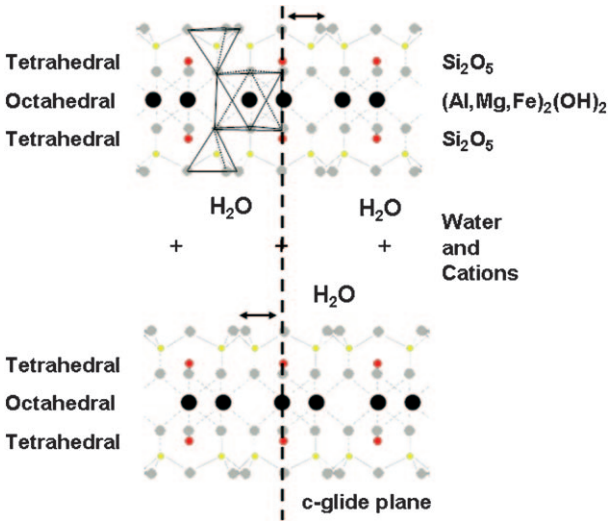

Figure 6. Scheme of a two-layer smectite, which indicates the shift of two adjacent layers view along *a*.

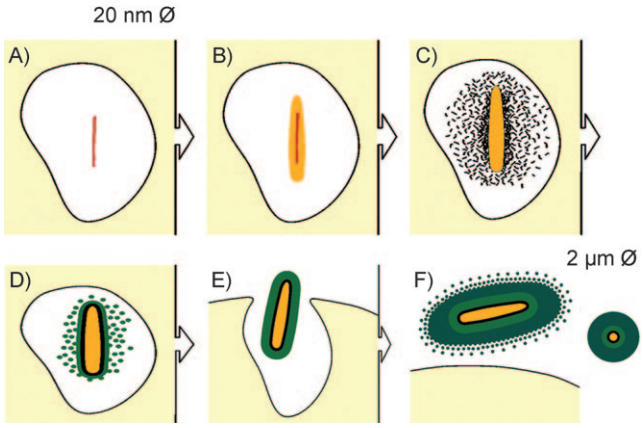

Figure 7. Scheme of spicule development stages; from the initial nanospicule (template) to the released extracellular mature spicule. First: the crystalline nanorods are synthesized (A), then the synthesis of the organic axial filament that contained silicatein proceeds around the nanorods (B, C). The synthesis of the first silica layer occurs and simultaneously the nanorod that has been used as template for axial filament growth disappears (C, D); The first silica layer has been completed (E), the intracellular formation of the spicules is completed and the spicules are extruded for the extracellular space (F).

sigmas with a regular banding pattern of 7 nm, but no further explanation was offered.[29] Later on, Simpson et al.[30] described in a cross section of a freshwater sponge—*Ephydatia muelleri*—also the presence of crystallinity on the axial filament, but, both of these authors reported paracrystallinity in mature spicules. Müller et al. described the presence of unusual and intracellular storage of silica rod crystals during the spiculogenesis of the freshwater sponges *E. muelleri* and *Spongilla lacustris*.[31]

Paracrystallinity of nanostructures located in the axial filament has been attributed to being responsible for shaping the axial filaments[32] from different sponge species, for example, a hexagonal shape in haplosclerid or triangular in poecilosclerid *Phorbas fictitius* and *tenacior*.[29,33,34] This question, however, remains speculative and unsolved. According to our results, it seems that the shape of the axial filament is given by a crystalline structure that acts like an intracellular seed/template that is subsequently layered by biopolymers and silicatein. Amorphous biosilica is then enzymatically formed concentrically around these axial filaments as the early step of spicule formation (Figure 7). The structure of these highly crystalline nanorods that are found in *S. domuncula* is resolved and shows a unique layered silicate smectite type. HRTEM analysis on the axial filament of *S. domuncula* did not show the presence of any crystalline structure; this suggests that the template disappears by an unknown mechanism.

The formation of biominerals is a very complex system, and the only aspects of them that have received attention are the interactions between the macromolecules (polysaccharide, polymers, proteins) and the inorganic materials (Ca, Si). Perry et al. showed the importance of the effect of inorganic species, such as Si and Al, in the biomineralization environment. The same author showed that Al and orthosilicic acid/silica are able to interact under conditions that are relevant to biological systems.[35,36] In complex biological systems, the codeposition of Si and Al is commonly found, and it seems to be an evolutionary mechanism as a protection against aluminum toxicity.[37,38] For example, it has been demonstrated that the pond snail *Lymnea stagnalis* up-regulates the internalization of Si when exposed to high concentrations of Al, thus forming a vacuolar lysosomal codeposition of Si and Al.[39] In the case of Demospongiae, the spicule-forming cells, sclerocytes, comprise special vesicles in which the primary stages of spicules proceed. The formation of these crystalline nanorods could be a result of the sponge's evolutionary protection mechanism against Al toxicity. The presence of Al in the intracellular crystalline structure can be attributed to the presence of a silicatein antagonist enzyme, silicase, which has already been described to be present in *S. domuncula*. This enzyme is colocalized with silicatein at the surface of the growing spicules, in the axial filament, and subsequently in the axial canal.[40] Silicase is a catabolic enzyme that catalyzes the decomposition of biosilica from sponge spicules; it releases to the medium Si and other trace metal compounds that can be reintegrated into the spicule-formation process. The presence of the Al, as well as other elements, in spicules from *S. domuncula* has been previously reported.[41] This assumption is confirmed by the absence of Al in all components that have been used for primmorphs growth, that is, artificial seawater and RPMI medium. Artificial seawater was analyzed by STEM-EDX, which confirmed the complete absence of any hydroxy-aluminosilicates polymers (HAS) or other silica-containing crystalline structures; this, in turn, excludes the possibility of formation, under these conditions, of exogenous HAS.

Conclusions

For the first time a crystalline structure was localized within the organic axial filament of the primordial spicules. We suggest that this crystalline structure acts as an inorganic template and gives shape and orientation to the newly forming spicule,

although its function is admittedly not yet fully understood. Experimental evidence has been presented that the silicatein molecules assemble to multimers in an ordered way by fractal patterning.[42,43] These associations, however, cannot solely be attributed to the axial filament formation because of the size of those structures.

TEM techniques clearly show their high applicability as tools to unveil the complex process of biomineralization. These techniques allowed us to shed a light on the early stages of spicule formation for the first time. Thanks to HRTEM, the crystalline nanorods that are localized intracellularly in sponge cells (sclerocytes) could be detected, thus moving one step closer to the starting point of spicule biosilicification. ADT allowed us to collect a sufficient data set from a single crystal (classified as being a typical smectite) to unambiguously determine the cell vectors, even in presence of defects and beam-sensitive material. How and where this crystalline structure originated, and whether it is a common feature in demosponges remains unknown. Studies are being performed to understand the origin of these crystalline structures.

Indeed, the use of sophisticated techniques and the multidisciplinary approach is necessary to understand the complexity of the fine interactions between the organic and inorganic compartments during biomineralization. These results might contribute to the understanding of biosilicification in sponges and might help to provide a new insight for bio-nanotechnological applications with a potential in the biomimetic and biomedical field.

Experimental Section

Primmorph cell culture: Live specimens of *S. domuncula* (Porifera, Demospongiae, Hadromerida) had been collected in the Adriatic Sea near Rovinj (Croatia) and had been kept in aquaria in Mainz, Germany, for over ten months at a temperature of 17 °C prior to their use. Single cells were obtained as described in Müller et al.[9] Briefly, tissue samples were cut into cubes and single cells were obtained by dissociation with Ca^{2+} and Mg^{2+}-free artificial seawater (CMFASW), that contained 2.5 mM EDTA.[44] The analysis of the filtered and dried CMFASW by using TEM and STEM-EDX did not show any ordered structure that contained silicon. The cell suspension was centrifuged, and the final pellet was resuspended in CMFASW that had been supplemented with 0.1% of RPMI 1640 medium (Biochrom AG, Berlin, Germany) and 60 μM silicic acid (as sodium metasilicate; Sigma–Aldrich). Primmorphs of at least 1 mm in diameter were formed after five days and used for the studies that are described here. Sponge samples were cut into pieces (2 mm^3), incubated in 0.1 M phosphate buffer that was supplemented with 2.5% gluteraldehyde, 0.82% NaCl (pH 7.4), and then washed in 0.1 M phosphate buffer (1.75% NaCl) at room temperature. After the samples had been treated with 1.25% $NaHCO_3$, 2% OsO_4, and 1% NaCl, they were dehydrated with ethanol. The dried samples were incubated with propylene oxide, fixed in propylene oxide/Araldite (2:1), covered with pure Araldite, and hardened at 60 °C for two days prior to being cut into 60 nm ultrathin slices (Ultracut S; Leica, Wetzlar, Germany).

Microscopy analysis: The samples were finally transferred onto copper grids (Plano, Wetzlar, Germany) coated with 1.2% Formvar. TEM analysis was carried out with a FEI Tecnai F30 S-TWIN transmission electron microscope equipped with a field emission gun and a scanning unit. STEM was performed by using the Tecnai Microprobe STEM mode with a focused beam of approximately 0.5 nm, and images were collected by a Fischione high-angular annular dark field detector (HAADF). Nano-electron diffraction (NED) was performed with a 10 μm C2 aperture to produce a 50 nm beam for a semiparallel illumination of the sample. High-resolution images (HRTEM) and NED patterns were taken with a CCD camera (14-bit GATAN 794MSC) and acquired by using Gatan DigitalMicrograph software.

Automated diffraction tomography (ADT) was carried out with a single tilt sample holder by using specific software that was developed for FEI Tecnai F30 TEM.[14] Two complete tilt series that consisted of 61 slides in the range between −30° and 30° with a step size of 1° were obtained. The software was able to track the position of the sample after each tilt step by using autocorrelation of a STEM image and to acquire NBD patterns, sequentially. The dose rate on the sample was kept at the level of approximately 3e/Å2s. For data processing, including 3D reconstruction, automated cell parameter determination software, which was self-programmed in Matlab was used.[15] Errors in cell axes were calculated as standard deviations of the distance between the cluster center and the refined vector positions. For visualization, UCSF Chimera software was used,[45] but the output files had standard MRC format and can be viewed by any appropriate visualizer.

Elemental analysis: Energy dispersive X-ray analysis (EDX) was undertaken in STEM mode and quantified by using FEI ES Vision software.

To determine via ICP-AES, the composition of mature spicules 48% HF (15 mL) and 97% 1+1 H_2SO_4 (1 mL) was added into a crucible and placed it onto an electric heating plate to evaporate the Si. When the crucible was almost dry 48% HF (5 mL) was added, and the silica was completely volatilized by evaporating the solution to dryness. Then it was placed in a cold, electric muffle furnace, and the procedures were repeated for the determination of LOI. The percentage of SiO_2 was obtained by the weight difference. To determine the other compositions extraction solvent of 37% 1+1 HCl (2 mL) was added to the above-described crucible, then transferred quantitatively to a 10 mL volumetric flask and dilute to volume. The Na_2O, MgO, Al_2O_3, K_2O, CaO, Fe_2O_3, and TiO_2 content was determined by ICP-AES (Thermo IRIS Advantage), and the other elements were determined by ICP-MS (Thermo VG PQ ExCell).

Acknowledgements

This work has been supported by the Deutsche Forschungsgemeinschaft under the auspices of the SFB 625. The authors thank Prof. Fernando Nieto, Departamento Mineralogia y Petrologia, Granada, Spain for fruitful discussion.

Keywords: bioinorganic chemistry · electron crystallography · nanostructures · silicatein · spicules

[1] E. Bäuerlein, *Handbook of Biomineralization, Vols. 1–3* (Eds.: E. Bäuerlein, P. Behrens, M. Epple), Wiley-VCH, Weinheim, **2007**.
[2] E. Bäuerlein, *Handbook of Biomineralization; Vol. 1: Biological Aspects and Structure Formation*, Wiley-VCH, Weinheim, **2007**.
[3] W. E. G. Müller, *Silicon Biomineralization: Biology-Biochemistry-Molecular Biology-Biotechnology*, Springer, Berlin, **2003**.
[4] M. J. Uriz, *Can. J. Zool.* **2006**, *84*, 322–356.

[5] K. Shimizu, J. Cha, G. D. Stucky, D. E. Morse, *Proc. Natl. Acad. Sci. USA* **1998**, *95*, 6234–6238.
[6] H. C. Schröder, A. Boreiko, M. Korzhev, M. N. Tahir, W. Tremel, C. Eckert, H. Ushijima, I. M. Müller, W. E. G. Müller, *J. Biol. Chem.* **2006**, *281*, 12001–12009.
[7] W. E. G. Müller, M. Rothenberger, A. Boreiko, W. Tremel, A. Reiber, H. C. Schröder, *Cell Tissue Res.* **2005**, *321*, 285–297.
[8] W. E. G. Müller, S. I. Belikov, W. Tremel, C. C. Perry, W. W. C. Gieskes, A. Boreiko, H. C. Schröder, *Micron* **2006**, *37*, 107–120.
[9] W. E. G. Müller, M. Wiens, R. Batel, R. Steffen, H. C. Schröder, R. Borojevic, M. R. Custodio, *Marine Ecol. Progr. Ser.* **1999**, *178*, 205–219.
[10] H. C. Schröder, F. Natalio, I. Shukoor, W. Tremel, U. Schloßmacher, X. Wang, W. E. G. Müller, *J. Struct. Biol.* **2007**, *159*, 325–334.
[11] O. Bütschli, *Z. Wiss. Zool.* **1901**, *69*, 235–286.
[12] D. L. Dorset, *Structural Electron Crystallography*, Plenum, New York, **1995**.
[13] U. Kolb, K. Büscher, C. Helm, A. Lindner, A. F. Thünemann, M. Menzell, M. Higuchi, D. G. Kurth, *Proc. Natl. Acad. Sci. USA* **2006**, *103*, 10202–10206.
[14] U. Kolb, T. Gorelik, C. Kübel, M. T. Otten, D. Hubert, *Ultramicroscopy* **2007**, *107*, 507–513.
[15] U. Kolb, T. Gorelik, M. T. Otten, *Ultramicroscopy* **2008**, *108*, 763–772.
[16] Cerius 2 version 4.2, Accelrys Inc., 9685 Scranton Road, San Diego, USA, 92121 – 93752.
[17] R. J. Merriman, D. R. Peacor in *Low-Grade Metamorphism* (Eds.: M. Frey, D. Robinson), Blackwell, Oxford, **1999**, pp. 10–60.
[18] S. I. Tsipursky, V. A. Drits, *Clay Miner.* **1984**, *19*, 177–193.
[19] N. Güven, *Rev. Mineral.* **1988**, *19*, 497–559.
[20] M. M. A. Drief, F. Nieto, *Clay Miner.* **2000**, *35*, 665–678.
[21] A. Sánchez-Navas, A. Martín-Algarra, F. Nieto, *Sedimentology* **1998**, *45*, 519–533.
[22] V. Donati, *Auszug seiner Natur-Geschichte des Adriatischen Meers*, Halle, CP Franckens, **1753**.
[23] H. J. Carter, *Ann. Mag. Natl. Hist.* **1849**, *4*, 81–100.
[24] M. J. Uriz, X. Turon, M. Becerro, *Cell Tissue Res.* **2000**, *301*, 299–309.
[25] K. Shimizu, J. Cha, G. D. Stucky, D. E. Morse, *Proc. Natl. Acad. Sci. USA* **1998**, *95*, 6234–6238.
[26] A. Krasko, R. Batel, H. C. Schröder, I. M. Müller, W. E. G. Müller, *Eur. J. Biochem.* **2000**, *267*, 4878–4887.
[27] T. L. Simpson, *The Cell Biology of Sponges*, Springer, New York **1984**.
[28] W. J. Sollas, *Report on the Tetractinnellida Collected by H.M.S. Challenger During the Years 1873–1876, Report on the Scientific Results of the Voyage of H.M.S. Challenger During the Years 1873–1876*, London, **1888**, pp. 47–50.
[29] C. R. Wilkinson, R. Garrone, *J. Morphol.* **1980**, *166*, 51–63.
[30] T. L. Simpson, R. Garrone, M. Mazzorana, *J. Ultrastruct. Res.* **1983**, *85*, 159–174.
[31] G. Imsiecke, W. E. G. Müller, *Cell. Mol. Biol.* **1995**, *41*, 827- 832.
[32] G. Croce, A. Frache, M. Milanesio, D. Viterbo, G. Bavestrello, U. Benatti, M. Giovine, H. Amenitsch, *Microsc. Res. Tech.* **2003**, *62*, 378–381.
[33] R. Garrone, *J. Microsc.* **1969**, *8*, 581–598.
[34] C. Donadey, J. Paris, J. Vacelet in *New Perspectives in Sponge Biology* (Ed.: K. Rützler), Smithsonian Institution, Washington D.C. **1990**, pp. 259–263, (from the International Conference on the Biology of Sponges, **1985**.)
[35] C. C. Perry, T. Keeling-Tucker, *J. Inorg. Biochem.* **2000**, *78*, 331–339.
[36] C. C. Perry, T. Keeling-Tucker, *J. Inorg. Biochem.* **1998**, *69*, 181–191.
[37] C. Exley, J. D. Birchall, *J. Theor. Biol.* **1992**, *159*, 83–98.
[38] J. D. Birchall, C. Exley, J. S. Chappell, M. J. Philips, *Nature* **1989**, *338*, 146/148.
[39] M. Desouky, R. Jugdaohsingh, C. R. McCrohan, K. N. White, J. J. Powell, *Proc. Natl. Acad. Sci. USA* **2002**, *99*, 3394–3399.
[40] C. Eckert, H. C. Schröder, D. Brandt, S. Perovic-Ottstadt, W. E. G. Müller, *J. Histochem. Cytochem.* **2006**, *54*, 1031–1040.
[41] F. Sandford, *Microsc. Res. Tech.* **2003**, *62*, 336–355..
[42] M. M. Murr, D. E. Morse, *Proc. Natl. Acad. Sci. USA* **2005**, *102*, 11657–11662.
[43] W. E. G. Müller, A. Boreiko, U. Schloßmacher, X. Wang, M. N. Tahir, W. Tremel, D. Brandt, J. A. Kaandorp, H. C. Schröder, *Biomaterials* **2007**, *28*, 4501–4511.
[44] W. E. G. Müller, J. Arendes, B. Kurelec, R. K. Zahn, I. Müller, *J. Biol. Chem.* **1997**, *252*, 3836–3842.
[45] UCSF Chimera package from the Resource for Biocomputing, Visualization, and Informatics at the University of California, San Francisco (supported by NIH P41 RR-01081).

Received: September 16, 2008
Published online on January 30, 2009

